FERMILAB-Conf-03/205-E March 2004

Recent Results in High p_T Physics from CDF

Gregory F. Veramendi

UC Berkeley / LBNL
e-mail: mendi@fnal.gov
(for the CDF Collaboration)

Abstract. We present the most recent high p_T results from the CDF experiment using $p\bar{p}$ collisions at $\sqrt{s} = 1.96$ TeV produced at the Tevatron Collider at Fermilab. We summarize results in electroweak physics, top physics and searches for physics beyond the Standard Model. Many measurements of important signals like W boson, Z boson, and the top quark have been reestablished. Taking advantage of the increase in energy and detector upgrades, these measurements already begin to be competitive with previous results.

PACS: 12.15.Ji, 12.15.Mm, 12.38.Qk, 12.60.-i, 13.38.-b, 13.85.-t, 14.65.Ha, 14.70.-e, 14.80.-j

1 Introduction

The Tevatron collider has undergone extensive upgrades over the last five years with the goal of increasing the instantaneous luminosity by over an order of magnitude and increasing the energy by 9%. Data taking began at both CDF and DØ experiments in early 2002, and the results presented in this paper represent the physics quality data taken by CDF through January 2003. The amount of data used in the following analyses range from 53–91 pb^{-1}, depending on what parts of the detector were used and when the analysis was finished. The CDF detector has undergone a considerable upgrade whereby the entire tracking system and forward ($1.0 < |\eta| < 3.6$) calorimeter detectors were replaced. The silicon tracking detector has been replaced to improve the coverage of the interaction region and to provide forward tracks to $|\eta| < 2$. A new time of flight (TOF) detector has been installed. The muon coverage has been increased to $|\eta| < 1.5$. The entire DAQ and trigger systems have been replaced with the additional capability of being able to trigger on drift chamber tracks with every bunch crossing, and trigger on displaced vertices at the second level of the trigger.

2 Recent results in electroweak physics

The electroweak program at CDF consists of making precision measurements of the properties of Z and W bosons created through $q\bar{q}$ annihilation. Most of the measurements use the electron and muon decays since they have the cleanest signatures. Tau decays are also considered, although they have higher backgrounds since they are more difficult to identify. The program consists of

baseline measurements such as the W and Z cross sections to the three different leptons that give us confidence in our understanding of the detector and analysis tools. Analyses to make precision measurements include the measurement of the Drell-Yan rapidity spectrum ($d\sigma_Z/dy$), the W charge asymmetry, the W mass, W width, and the W polarization. Finally, we can put constraints on new physics by looking for anomalous couplings in diboson production, and looking at the Drell-Yan mass and forward-backward asymmetry spectrums for deviations from the Standard Model.

2.1 W and Z cross sections

The W and Z cross sections serve as our "standard candles" for all of the high p_T analyses. They have low backgrounds and relatively high cross sections so the measurements are already systematics limited. The W cross section is important because it leads into many of the precision measurements involving the W boson, and may be used to normalize future cross section measurements. The W and Z samples are used to understand detector and object identification efficiencies, and to develop new analysis techniques. They use the inclusive high p_T lepton triggers ($W \to \tau\nu_\tau$ analysis uses a large $\not\!\!E_T$ trigger) which are the principal triggers for most electroweak analyses, top analyses and many analyses searching for new physics. The leptonic signature of the W is large $\not\!\!E_T$ and a central isolated high p_T lepton. The leptonic signature of the Z is two central isolated high p_T leptons. The candidate event yield in each channel, background fraction and measured cross section for W and Z decaying to different leptons in 72 pb^{-1}of Run II data is shown in Table 1. The cross sections can be compared with the NNLO predictions [1] of 2.731±0.002 nb and 250.5±3.8 pb for W and Z production respectively. Figure 1 shows the transverse mass distribution for $W \to \mu\nu_\mu$, which will be an important contribution to the W mass measurement, and the invariant mass distribution for $Z \to e^-e^-$, which is important for understanding the energy/momentum scale and resolution. Figure 2 shows the W and Z cross section measurements compared with the NNLO prediction [1]. The $W \to \tau\nu_\tau$ cross section measurement is considered the baseline measurement for analyses using τ's. Figure 3 shows the track multiplicity of $W \to \tau\nu_\tau$ candidates and is a benchmark for detector efficiencies and background estimation. Analyses using τ's are still being optimized and we expect to gain a factor of two in yield from optimizations in the trigger and analysis techniques. This will be important for SUSY Higgs searches where $tan\beta$ is large and the decay $A/h \to \tau\tau$ is enhanced [2].

2.2 Γ_W and lepton universality

Taking the ratio of the Z and W cross sections, we compute the ratio $R_\ell = \sigma_W Br(W \to \ell\nu_\ell)/\sigma_Z Br(Z \to \ell^+\ell^-)$ for electrons and muons. The results for the electron and muon analyses are shown in Table 2. They agree well with the NNLO calculation of 10.66 ± 0.05 [1]. Using the LEP measurement [3] of $\mathrm{Br}(Z \to e^+e^-)$ and theoretical predictions for σ_W/σ_Z and $\mathrm{Br}(W \to e\nu_e)$, the measurement of R_e can be used to indirectly measure Γ_W. The results for using

Table 1. The event yield, background fraction, and measured cross sections for the W and Z analyses using 72 pb^{-1} of Run II data.

Channel (ℓ)	Sample	Background	σ·Br
$W \to e\nu_e$	38625	6%	$2.64 \pm 0.01_{stat} \pm 0.09_{sys} \pm 0.16_{lum}$ nb
$W \to \mu\nu_\mu$	21599	11%	$2.64 \pm 0.02_{stat} \pm 0.12_{sys} \pm 0.16_{lum}$ nb
$W \to \tau\nu_\tau$	2345	26%	$2.62 \pm 0.07_{stat} \pm 0.21_{sys} \pm 0.16_{lum}$ nb
$Z \to e^+e^-$	1830	0.6%	$267 \pm 6_{stat} \pm 15_{sys} \pm 16_{lum}$ pb
$Z \to \mu^+\mu^-$	1631	0.9%	$246 \pm 6_{stat} \pm 12_{sys} \pm 15_{lum}$ pb

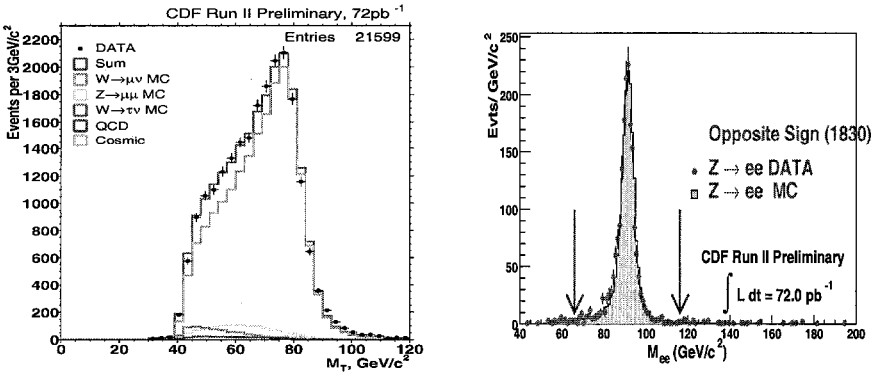

Fig. 1. Transverse mass distribution of $W \to \mu\nu_\mu$ candidates (left) and the invariant mass distribution of $Z \to e^+e^-$ candidates collected in 72 pb^{-1} of Run II data.

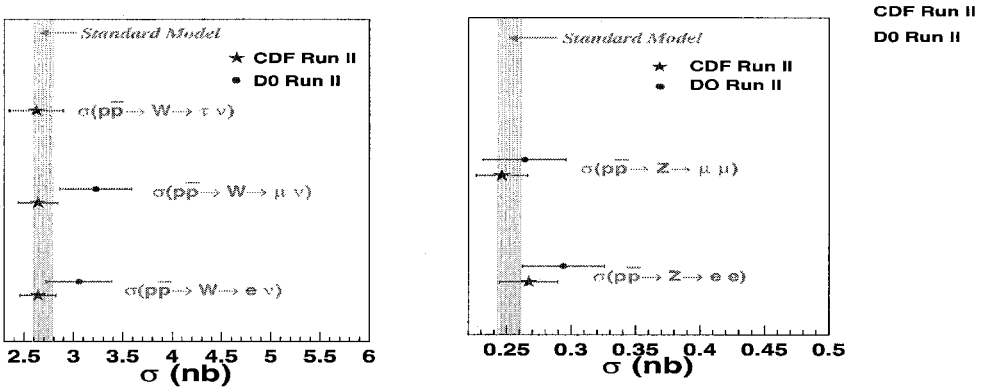

Fig. 2. Comparisons of cross section measurements for W (left) and Z (right) bosons with NNLO calculations from CDF and DØ using Run II data.

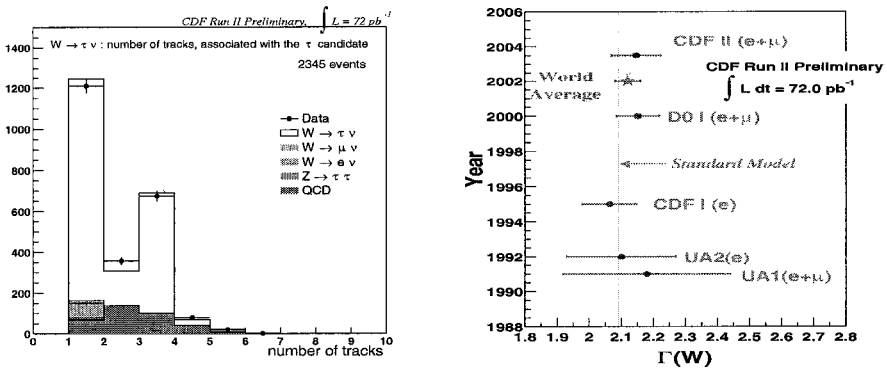

Fig. 3. The track multiplicity of $W \to \tau\nu_\tau$ candidates compared with predictions of background and signal simulation(left). A comparison of results of indirect measurements of Γ_W (right)

Table 2. Results of the ratio $R_\ell = \sigma_W Br(W \to \ell\nu_\ell)/\sigma_Z Br(Z \to \ell^+\ell^-)$, and Γ_W from R_ℓ using 72 pb^{-1} of Run II data.

sample	R_ℓ	Γ_W (GeV/c^2)
e	$9.88 \pm 0.24_{stat} \pm 0.47_{sys}$	$2.29 \pm 0.06_{stat} \pm 0.10_{sys}$
μ	$10.69 \pm 0.27_{stat} \pm 0.33_{sys}$	$2.11 \pm 0.05_{stat} \pm 0.07_{sys}$
combined	$10.54 \pm 0.18_{stat} \pm 0.33_{sys}$	$2.15 \pm 0.04_{stat} \pm 0.07_{sys}$

electrons, muons, and combining the two measurements are shown in Table 2. Figure 3 compares that determination to previous indirect measurements of the W boson width. Again, the results agree well with the theoretical calculation in [4] ($\Gamma_W = 2.067 \pm 0.021$ GeV/c^2). The electron and τ cross sections can be combined to test lepton universality by extracting the ratio of coupling constants, $g_\tau^W/g_e^W = 0.99 \pm 0.04_{stat} \pm 0.07_{sys}$.

2.3 Forward-Backward asymmetry using dielectrons

The presence of both vector and axial-vector couplings of electroweak bosons to fermions in the process $\bar{q}q \to Z/\gamma \to \ell^+\ell^-$ gives rise to an asymmetry in the polar angle of the electron momentum in the rest frame of the lepton pair. If the number of forward events, N_F, is defined as the number of events with positive $\cos\theta$ and the number of backward events, N_B, as the number of events with negative $\cos\theta$, then the forward-backward charge asymmetry A_{FB} is:

$$\begin{aligned} A_{FB} &= \frac{N_F - N_B}{N_F + N_B} \\ &= \frac{\sigma(\cos\theta > 0) - \sigma(\cos\theta < 0)}{\sigma(\cos\theta > 0) + \sigma(\cos\theta < 0)} \end{aligned}$$

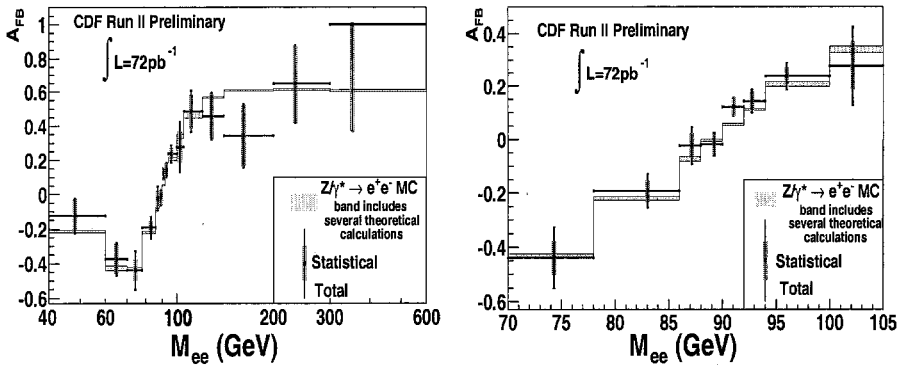

Fig. 4. The forward-backward asymmetry of electron-positron pairs measured by CDF, compared to theory predictions. The results are shown for the entire m_{ee} spectrum (left) and for events near the Z pole (right).

(1)

and A_{FB} is a direct probe of the relative strengths of the vector and axial-vector couplings over the range of Q^2 being considered. In addition, A_{FB} constrains the properties of any additional non-Standard Model amplitudes contributing to $q\bar{q} \to \ell^+\ell^-$, and is complementary to a direct search for them via excesses in the total cross section.

Although it will be very difficult for the Tevatron to compete with LEP measurements for Q^2 below 200 GeV, the Tevatron can probe beyond the energies that were available at LEP. The A_{FB} measurement takes advantage of both the central and forward calorimeters identifying isolated high p_T electrons out to $|\eta| < 3$. We find 5438 candidate events with $40 < M_{ee} < 600$ GeV/c^2 using 72 pb^{-1} of data. The background, which comprises about 3% of the sample, is dominated by dijet production. The dependence of A_{FB} with M_{ee} is shown in Figure 4. Results agree with theoretical predictions.

2.4 W Charge Asymmetry

Theoretical uncertainty on the parton density functions of the proton is a significant error in many measurements at the Tevatron, such as the W mass. Measurement of the forward-backward charge asymmetry in $p\overline{p} \to W^{\pm}$ provides a constraint on these parton fluxes. Since u quarks carry, on average, a higher fraction of the proton momentum than d quarks, W^+ produced by $u\overline{d} \to W^+$ tend to be boosted in the proton direction. Similarly, W^- tends to be boosted in the anti-proton direction. This results in a non-zero forward-backward charge asymmetry defined as:

$$A(y_W) = \frac{d\sigma(W^+)/dy - d\sigma(W^-)/dy}{d\sigma(W^+)/dy + d\sigma(W^-)/dy} \tag{2}$$

where y is the rapidity of the W bosons and $d\sigma(W^{\pm})/dy$ is the differential cross section for W^+ or W^- boson production.

Leptonic decays of the W boson, in our case $W \to e\nu_e$, provide a cleanly identified sample for studying this asymmetry. The p_z of the neutrino is unmeasured but can be determined with a W mass constraint, up to a two-fold ambiguity. In some cases, where that ambiguity can be reduced due to the known V-A decay distribution in the W rest frame, y_W can provide a direct measure of the W production asymmetry. Initially however, we use the experimentally more direct $e^{\pm}$ direction to measure the forward-backward electron asymmetry,

$$A(\eta_e) = \frac{d\sigma(e^+)/d\eta - d\sigma(e^-)/d\eta}{d\sigma(e^+)/d\eta + d\sigma(e^-)/d\eta} \tag{3}$$

which convolves the W production asymmetry with the V-A density distribution. It provides sensitivity to the ratio of the parton density functions for u and d quarks, $u(x)/d(x)$. This sensitivity is most pronounced at high values of $|\eta|$ (forward/backward region) as show in Figure 5. Thus the primary experimental challenge in this measurement is tracking in the forward region to obtain charge identification for electrons.

A new technique for tracking forward electrons has been developed for this purpose. The technique uses high energy electromagnetic clusters in the forward calorimeter to seed tracks through the silicon detector. Using the event vertex and the centroid of the shower in the calorimeter as two end points, the energy deposited in the calorimeter is used to predict two trajectories for the candidate electron depending on whether it is positively or negatively charged. A search for hits in the silicon detector along the two trajectories indicates whether an electromagnetic cluster is likely to be an electron and the better match of the two trajectories indicates the charge of the electron. The performance of this method is shown in Figure 5, where the efficiency is constant for $|\eta| < 1.8$. We expect results from this analysis in summer 2003. The sensitivity of the measurement using the forward tracking is shown in Figure 5, where the points are set to zero asymmetry, but the error bars indicate the expected uncertainty with 110 $\text{pb}^{-1}$of Run II data compared to the uncertainties from Run I. The extended reach of the Run II measurement is due to the improved forward tracking detector and calorimeter.

2.5 $W\gamma$ and $Z\gamma$ cross section

The interest in $W\gamma$ and $Z\gamma$ production in $p\bar{p}$ collisions arises from the sensitivity to the triple gauge-boson vertex. The value of this coupling is predicted from the electroweak $SU(2)_L \times U(1)_Y$ symmetry and measurements provide fundamental test of the non-Abelian nature of the Standard Model. Within the Standard Model the photon couples at the $WW\gamma$ vertex while the triple gauge-boson vertex for $ZZ\gamma$ coupling is predicted to be zero. If the W and Z bosons were to have internal structure, deviations from these Standard Model predictions would be observed. Limits on any non Standard Model contributions to $W\gamma$ and $Z\gamma$ production are usually placed in terms of so-called anomalous couplings $\Delta\kappa$ and λ which are zero in the Standard Model.

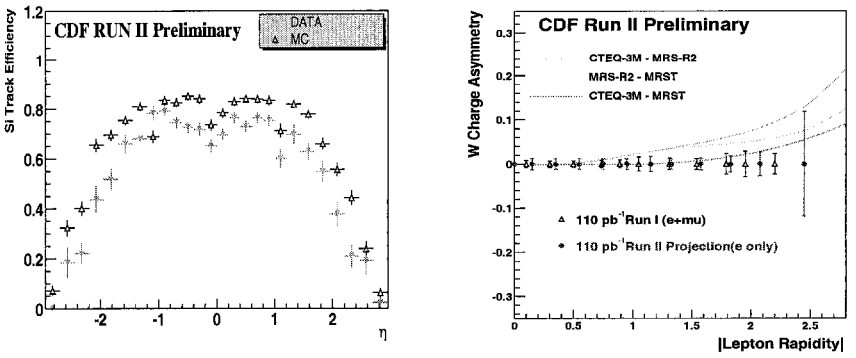

Fig. 5. Left: The track finding efficiency for the calorimeter seeded tracking method versus electron η. Right: The W charge asymmetry versus electron rapidity for various PDF's. Also the uncertainties from measuring the W charge asymmetry versus electron rapidity using 110 $pb^{-1}$of data from the Run I measurement, and the expected uncertainties using the Run II detector, where the central value is set to zero asymmetry.

Both the W and Z boson production can occur with direct photons from the bremsstrahlung of the initial state quarks and the boson's leptonic decay products. A full calculation of the $p\bar{p}$ production of W and Z bosons with direct photons must include these radiated photons in addition to those directly coupled to the W or Z boson vertex. Measurements of the triple gauge-boson couplings have been made at LEP in e^+e^- collisions and at the Tevatron in Run I.

Using 72 pb^{-1} of Run II data, we measure the cross sections for $W\gamma$ and $Z\gamma$, where $Z \to e^+e^-$ or $Z \to \mu^+\mu^-$ and $W \to e\nu_e$ or $W \to \mu\nu_\mu$. The selection is very similar to the W and Z cross section measurements, except there is an additional requirement of a hard photon ($E_T^\gamma > 7$GeV, $|\eta| < 1$) which is isolated from the leptons ($\Delta R(\gamma - \ell) > 0.7$). The dominant background in these measurements is dijet production. The measured total production cross section along with the theoretical prediction is shown in Table 3. All measurements are in good agreement with the theoretical predictions. In order to place constraints on anomalous couplings the total cross section and the kinematic distributions of the event sample are used. Figures 6 and 7 show kinematic distributions of $W\gamma$ events and $Z\gamma$ events respectively which will be used to place constraints on anomalous couplings in the future.

2.6 Diboson: WW

Heavy di-boson (WW, WZ, and ZZ) measurements will be important in Run II for a number of reasons. At the very least, much more precise measurements of the cross sections for these processes will be possible compared to Run I, leading to new limits on anomalous triple gauge boson couplings. Di-boson production is an important background in many Standard Model measurements, such as

Table 3. The event yield, background fraction, and measured cross sections for the $W\gamma$ and $Z\gamma$ analyses using 72 pb^{-1} of Run II data. The Standard Model theoretical prediction is shown as the first line in each case.

Decay Lepton (ℓ)	Candidate Sample	Background Fraction	σ·Br (pb)
$W\gamma \to \ell\nu_\ell\gamma$(th.)			18.7 ± 1.3
$W\gamma \to e\nu_e\gamma$	43	33%	$17.2 \pm 3.8_{stat} \pm 2.8_{sys} \pm 1.0_{lum}$
$W\gamma \to \mu\nu_\mu\gamma$	38	29%	$19.8 \pm 4.5_{stat} \pm 2.4_{sys} \pm 1.2_{lum}$
$Z\gamma \to \ell^+\ell^-\gamma$ (th.)			5.4 ± 0.4
$Z\gamma \to e^+e^-\gamma$	11	4.6%	$5.5 \pm 1.7_{stat} \pm 0.6_{sys} \pm 0.3_{lum}$
$Z\gamma \to \mu^+\mu^-\gamma$	14	4.0%	$6.0 \pm 1.6_{stat} \pm 0.7_{sys} \pm 0.4_{lum}$

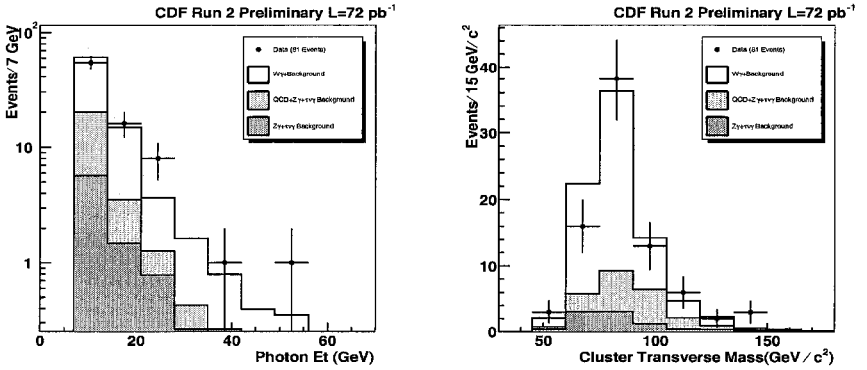

Fig. 6. Kinematic distributions from $W\gamma$ events using 72 pb^{-1}of Run II data. The photon E_T spectrum (left) and the transverse mass (right).

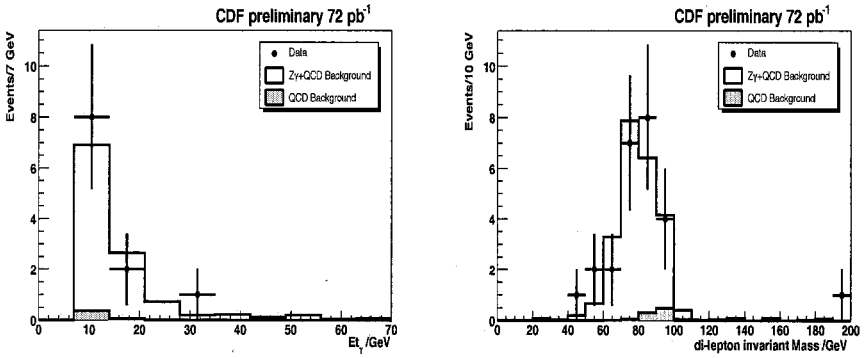

Fig. 7. Kinematic distributions from $Z\gamma$ events using 72 pb^{-1}of Run II data. The photon E_T spectrum (left) and the invariant mass (right).

Table 4. The signal prediction, background estimate, and number of $WW \to \ell\ell\nu_\ell\nu_\ell$ candidate events found in 72 pb^{-1} of Run II data.

Source	ee	$\mu\mu$	$e\mu$	$\ell\ell$
Backgrounds	0.29 ± 0.13	0.46 ± 0.18	0.77 ± 0.60	1.52 ± 0.64
$WW \to \ell\ell\nu_\ell\nu_\ell$	0.54 ± 0.12	0.65 ± 0.14	1.55 ± 0.34	2.74 ± 0.59
Data	1	0	1	2

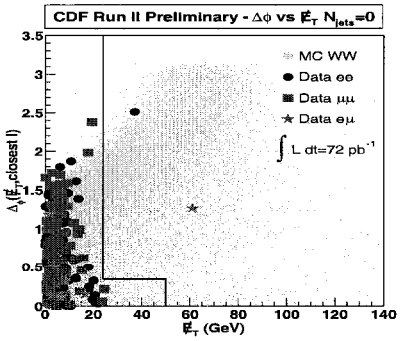

Fig. 8. WW candidates found in 72 pb^{-1} in the plane $\Delta\phi(\not\!\!E_T,\ell)$ versus $\not\!\!E_T$.

studies of top pairs using dilepton decays, and searches for physics beyond the Standard Model. In addition, being able to understand and control the di-boson signal will be a crucial step towards the possible discovery of the Higgs bosons. The $(W/Z)+Z$ di-boson channel with $Z \to b\bar{b}$ will provide a good calibration for $(W/Z)+H$ production with $H \to b\bar{b}$. For higher mass Higgs bosons, where WW^* decays become important, direct di-boson production must be understood as a contribution to the background. We have started looking for WW decay to dileptons in 72 pb^{-1} by selecting events with two oppositely charged high p_T leptons ($\ell = e, \mu$), $\not\!\!E_T$>25 GeV, and no additional jets in the event. Two events have been found ($e\mu, ee$), when we expect 2.7 ± 0.6 WW signal events and 1.5 ± 0.6 background events (see Table 4). So far the results are consistent with the Standard Model predictions, but we do not yet have enough data to make a cross section measurement. Figure 8 shows the kinematic distribution of the two events along with the Monte Carlo prediction.

3 Recent results in top physics

The top physics program at CDF consists of making precise measurements of top quark properties and production. Preliminary measurements of the top quark cross section have been made. The cross section measurements are interesting because they test the prediction of perturbative QCD, are sensitive to new physics beyond the Standard Model, and will be an important background in Higgs

searches. A very preliminary measurement of the top mass in the lepton plus jets sample has been made. This will continue to be an exciting measurement because of its ramifications for electroweak fits of the Standard Model Higgs boson mass. As the Tevatron accumulates more data than Run I, the precision top quark measurements begin in earnest with measurements of decay modes, branching ratios, searches for rare and non-Standard Model decays, and measurements of the $t\bar{t}$ production kinematics.

3.1 Top production and decay

At the current Tevatron energies, top quarks are produced mainly in pairs through the strong force mediated processes $q\bar{q} \rightarrow t\bar{t}$ (85%) and $gg \rightarrow t\bar{t}$ (15%). Top quarks can also be produced singly via the electroweak vertex $W \rightarrow tb$, but with half of the cross section of the QCD production. The increase in center of mass energy over Run I boosts the $t\bar{t}$ cross section by about 30%.

Within the Standard Model the top quark decays as a free quark, almost always to a W and a b quark. The decays and their respective signatures in the detector are categorized by how the W decays. The dilepton signature, where there are two leptons ($\ell = e, \mu$), two b jets, and $\not\!\!E_T$, corresponds to about 5% of the total cross section and has a low background. The "lepton plus jets" signature, where there is one lepton ($\ell = e, \mu$), four jets (two from b quarks) and $\not\!\!E_T$, comprises about 30% of the total cross section, but has a higher background. Finally, the "all-hadronic" signature, where there are 6 jets (two from b quarks), comprises about 44% of the total cross section, but has the highest backgrounds.

3.2 Dilepton cross section

Dilepton $t\bar{t}$ events are selected by requiring two high p_T isolated leptons from the two W's ($E_T^\ell > 20$ GeV), $\not\!\!E_T > 20$ GeV from the corresponding neutrinos, and two jets ($E_T^j > 10$ GeV, $|\eta_j| < 2$) from the b quarks. We also require that if the direction of the $\not\!\!E_T$ is near the direction of a jet or lepton, we increase the $\not\!\!E_T > 50$ GeV, to reduce the background from mis-measured energy faking the $\not\!\!E_T$ signature. Finally, a scalar sum of the transverse energy (H_T) of the leptons, jets, and $\not\!\!E_T$ is required to be greater than 200 GeV. With these cuts the signal to background ratio is 9/1, and we expect roughly 2.5 events. In 72 pb^{-1} , five candidates are found where 0.3 ± 0.12 background events are expected (see Table 5). The cross section is measured to be $\sigma_{t\bar{t}} = 13.2 \pm 5.9_{stat} \pm 1.5_{sys} \pm 0.8_{lum}$ pb, compared to the NLO theoretical prediction [5] of $\sigma_{t\bar{t}}(\sqrt{s} = 1.96 \text{ TeV}) = 6.7^{+0.71}_{-0.88}$ pb. Figure 9 shows the dilepton candidates and the expected $t\bar{t}$ theoretical prediction (with $M_{top} = 175$ GeV/c^2).

3.3 Lepton + jets cross section

Lepton plus jets $t\bar{t}$ events are selected by requiring one high p_T isolated central lepton from one of the W's ($E_T^\ell > 20$ GeV), $\not\!\!E_T > 20$ GeV, and at least three jets ($E_T^j > 15$ GeV, $|\eta_j| < 2$). Cosmic rays, photon conversions, Drell-Yan, and $t\bar{t}$ dilepton events are removed. At this point the signal to background ratio is

Table 5. The signal prediction, background estimate, and number of dilepton ($t\bar{t} \to \ell\ell\nu_\ell\nu_\ell b\bar{b}$) candidate events found in 72 pb^{-1} of Run II data.

Source	ee	$\mu\mu$	$e\mu$	$\ell\ell$
Backgrounds	0.10 ± 0.06	0.09 ± 0.05	0.10 ± 0.04	0.30 ± 0.12
$t\bar{t} \to \ell\ell\nu_\ell\nu_\ell b\bar{b}$	0.5 ± 0.05	0.59 ± 0.07	1.44 ± 0.16	2.5 ± 0.3
Data	1	1	3	5

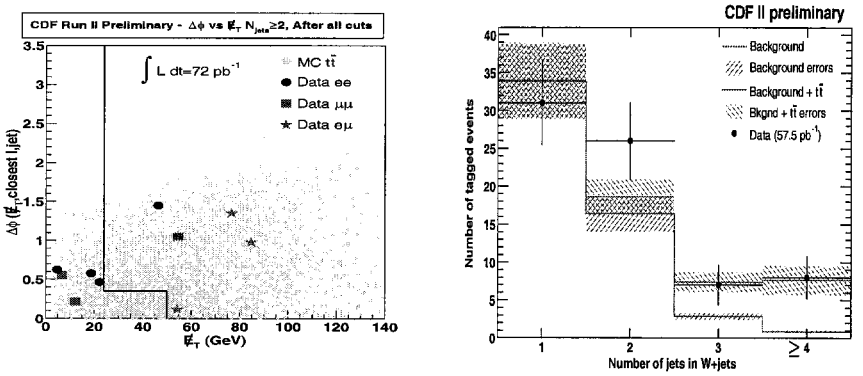

Fig. 9. The five dilepton $t\bar{t}$ candidate events found in 72 pb^{-1} in the plane $\Delta\phi(\not\!\!E_T,\ell)$ versus $\not\!\!E_T$(left). The number of events in the lepton plus jets sample with at least one b-tag (right): the 3 and $\geq$4 jet bins are used to extract $\sigma_{t\bar{t}}$.

Table 6. The signal prediction, background estimate, and number of lepton plus jets ($t\bar{t} \to \ell\nu_\ell b\bar{b}\ q\bar{q}$) candidate events found (before and after displaced vertex b-tagging) in 57.5 pb^{-1} of Run II data.

Source	$W+1$ jet	$W+2$ jets	$W+3$ jets	$W+\geq 4$ jets
Background	33.8 ± 5.0	16.4 ± 2.4	2.88 ± 0.5	0.87 ± 0.2
SM Background plus $t\bar{t}$	34.0 ± 5.0	18.7 ± 2.4	7.4 ± 1.4	7.6 ± 2.0
Data before tagging	4913	768	99	26
Data (≥ 1 b-tag)	31	26	7	8

1/6. To further reduce the background we use the silicon detector to identify a displaced vertex associated with a b jet. This improves the signal to background to 3/1. Using 57.5 pb^{-1} of Run II data we find 15 candidate events, with an expected non-$t\bar{t}$ background of 3.8 $\pm$ 0.5 events (see Table 6). Figure 9 shows expected signal and background contributions along with the number of candidate events. The events with only one or two jets are used as a control sample for our background prediction. The events in the three and four jet channels are used to measure the $t\bar{t}$ cross section. We measure the cross section in the lepton plus jets channel to be $5.3 \pm 1.9_{stat} \pm 0.8_{sys} \pm 0.3_{lum}$ pb, which agrees well with the NLO theoretical prediction [5] of $\sigma_{t\bar{t}}(\sqrt{s} = 1.96 \text{ TeV}) = 6.7^{+0.71}_{-0.88}$ pb.

3.4 Top mass

The top mass has been measured with the lepton plus $\geq$ four jet sample without requiring a displaced vertex associated with a b jet. In 72 pb^{-1} we find 33 candidate events. This method involves a constrained fit of the kinematics at the parton level. There are 24 possible combinations, 12 from the parton-jet matching and two possible longitudinal momenta for the neutrino. We perform a constrained-fitting technique (2-C fit) where we require energy-momentum conservation at production and decay vertices, the mass of the two top quarks be equal, and that the two jets, and the lepton and neutrino, assigned to the decays of the W bosons have the invariant mass of the W boson. This over-constrains the system of equations, and we calculate the χ^2 for each combination and choose the combination with the lowest χ^2. Mass templates are made by performing the same algorithm on $t\bar{t}$ Monte Carlo generated in 5 GeV/c^2 steps between 150 and 200 GeV/c^2 . A continuous likelihood method is used with parameterized mass templates, where the minimum of the likelihood distribution gives the central value for the top mass. Performing this on the 33 candidate events we measure a top mass of $171.2 \pm 13.4_{stat} \pm 9.9_{sys}$ GeV/c^2 . Figure 10 shows the 33 candidate events along with the signal and background templates, and the upper right-hand corner shows the output of the continuous likelihood fit. Being a first preliminary results, the systematic uncertainty is rather large, and is dominated by the jet energy scale uncertainty. This will improve as we continue to understand our detector better.

If we require a displaced vertex associated with a b jet, the measurement can

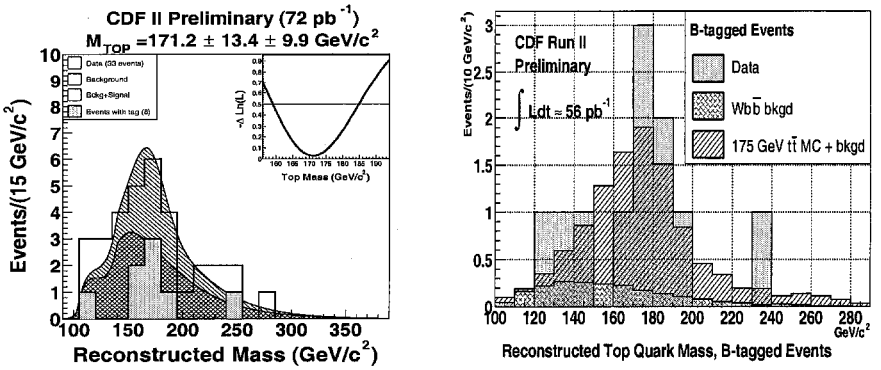

Fig. 10. The top mass distributions for events with no b-tag with 72 pb^{-1} of data(left), and with a b-tag with 56pb^{-1} of data(right). The events with no b-tag have been used to measure the top mass using a continuous likelihood method (left figure: top right inset).

be greatly improved. The b-tag identifies one of the jets as a b jet and reduces the number of combinations from 24 to 12. It also reduces the background. This improves the mass resolution. A preliminary look at this method is made in Figure 10. Since the b-tag reduces the background, the kinematic requirement on the fourth jet can be relaxed, and we find 11 candidate events in 56 pb^{-1} . We expect to have a measurement using b-tags by summer 2003.

4 Recent results in searches for physics beyond the Standard Model

The new phenomena program at CDF consists of searching for new objects at and above the electroweak scale. There are two approaches for searches at CDF. The model driven approach has the advantage of being able to optimize the analysis for a specific signature, but suffers because of the large number of possible models. Results presented such as searches for Leptoquarks, and doubly charged Higgs are examples of the model driven approach. The signature driven approach looks for new physics by choosing a well understood final state and comparing it to the Standard Model prediction. The signature driven approach has the advantage of testing many different models, but cannot be optimized for a specific signature. Results presented such as searches in the dijet spectrum, in diphoton final states, in high mass dilepton final states and for long-lived massive charged particles are examples of the signature driven approach. Many of the preliminary Run II results already surpass the limits set in Run I.

4.1 Searches for excited electrons

We have set a limit on excited electrons which are expected in many compositeness models. We use a model for excited fermions based on their coupling

to quarks and leptons via contact interaction that is described by an effective four-fermion Lagrangian [6] to set a mass limit. Requiring the e^* mass be equal to the compositeness scale, we set the 95% CL lower limit on the mass of an excited electron at 785 GeV/c^2 .

4.2 Searches for first generation Leptoquarks

Leptoquarks are hypothetical color-triplet particles carrying both baryon and lepton quantum numbers and are predicted by many extensions of the Standard Model as new bosons coupling to a lepton-quark pair [7]. Their masses are not predicted. They can be scalar particles (spin 0) or vector (spin 1) and at high energy hadron colliders they would be produced directly in pairs mainly through gluon fusion or quark antiquark annihilation. In most models Leptoquarks are expected to couple only to fermions of the same generation in order to avoid flavor-changing neutral current constraints. These analyses focus on the search for pair produced first generation scalar Leptoquarks S1 decaying either into eejj or ee$\nu\nu$. A search for first generation Leptoquarks decaying into two central electrons ($E_T^e > 5$ GeV) and two jets ($E_T^{(j_1,j_2)} > (30, 15)$ GeV) has been made using 72 pb^{-1} of Run II data. Zero events were found with an expected background of 3.4 ± 3 events. By assuming Br($LQ \to lq$) = 1, and using a NLO theoretical estimate, a 95% CL upper limit can be set on the production cross section as a function of Leptoquark mass (Figure 11(left)). First generation scalar Leptoquark with mass below 230 GeV/c^2 is excluded (the Run I limit was 220 GeV/c^2). Another analysis searching for Leptoquarks looked for Leptoquarks which decay to neutrinos and 2 jets. Events are selected by requiring 2 high E_T jets ($E_T^{(j_1,j_2)} > (45, 20)$ GeV) and $\not\!\!E_T$>55 GeV. Applying these cuts to 76 pb^{-1} of data we find 42 events with an expected background of 43$\pm$11 events. We set a 95% CL limit on the mass of the first generation Leptoquark ($LQ \to \nu q$), excluding the mass range $60 < m(LQ) < 107$ GeV/c^2 (Figure 11(right)).

4.3 Search for doubly-charged Higgs

Doubly-charged Higgs particles are members of Higgs triplets that occur in three types of models: models with extensions to the Higgs sector of the SM [8], left-right symmetric models [9], and supersymmetric left-right symmetric models [10]. The see-saw mechanism, designed in the context of the left-right symmetric model, successfully predicts light neutrino masses, and hence gives motivation for searching for doubly-charged Higgs bosons. 95 pb^{-1} of Run II data has been searched for same-sign central electron pairs above the Z pole. Events below the Z pole are used as a control sample for testing the background estimate. When searching in bins of $\pm$10% around each Higgs mass considered, no events are observed, and 95% CL upper limits on the cross section are set (Figure 12(left)).

4.4 Search for long-lived massive charged particles

Physics theories extending the Standard Model usually predict new conserved quantum numbers leading to stable particles. Long-lived CHArged Massive ParticleS (CHAMPS) escaping the CDF detector can be detected by high-p_T muon

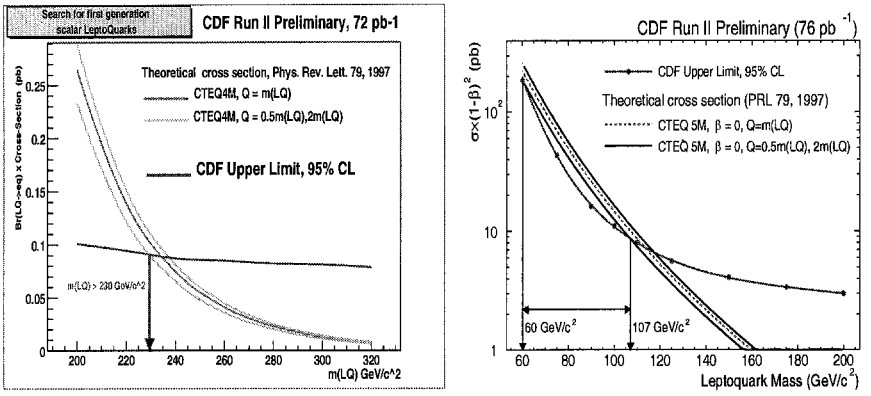

Fig. 11. 95% CL upper limit cross section as a function of Leptoquark mass compared with NLO theoretical expectations for Leptoquarks that decay to leptons and quarks (left), and for Leptoquarks that decay to neutrinos and quarks (right).

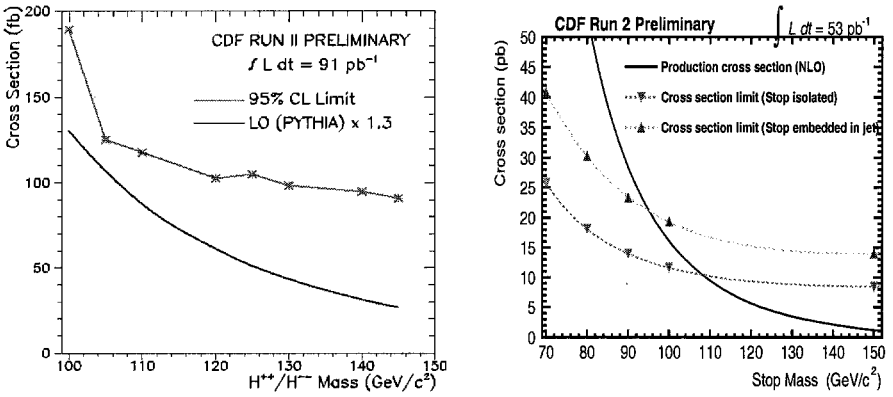

Fig. 12. 95% CL upper limit on $\sigma \cdot \mathrm{Br}(ee)$, as a function of doubly-charged Higgs mass, compared to theoretical expectation (left). 95% CL upper limit on the cross section for for isolated and non-isolated stable stops compared with NLO theoretical prediction (right).

triggers. Moreover, due to their large mass, these particles are expected to move slowly, leading to long Time-Of-Flight (TOF) through the detector. CHAMP production has been investigated by exploiting the new TOF system, providing sensitivity to higher $\beta\gamma$ values than the dE/dx measurement used in Run I analyses. 53 pb^{-1} of high-p_T muon data have been used. In order to have full tracking efficiency on CHAMPS with mass larger than 100 GeV/c^2 , a cut at 40 GeV/c is applied on the transverse momentum of the candidate tracks. The time t_0 at which the interaction occurred is estimated by averaging the measured time for tracks with $p_T <$ 20 GeV/c. Tracks with high time of flight difference Δt with respect to the t_0 are looked for. In 53 pb^{-1} of Run II data 7 events are observed where $2.9\ ^{+3.2}_{2.0}$ events are expected. Production cross section upper limits are established for a stable stop model [11](Figure 12 (right)). By assuming NLO predictions, a 95% CL lower limit on the stop mass is set at 108 GeV/c^2 , where the stop is isolated in the detector. The lower limit on the mass for a stop embedded in a jet is 95 GeV/c^2 .

4.5 Search for new particles decaying to dijets

Many classes of new particles have a larger branching fraction into just two partons (quarks and gluons) than into modes containing a lepton or electroweak gauge boson. Frequently this channel (dijets) is not searched because of the large QCD dijet background and the poor mass resolution. However, high statistics in the dijet sample allow exclusions of cross sections that are a small fraction of the dijet cross section. New particles with a natural width significantly smaller than the measured dijet mass resolution should all appear as a dijet mass resonance of the same line shape in our detector. Thus the poor dijet mass resolution allows us to search for many different phenomena with a single measured distribution. When setting $\sigma \cdot Br$ upper limits, we only need to model the resonance shape for a single type of particle decaying to dijets. We can then compare this cross section upper limit to the predicted cross section versus mass of any particle with a narrow intrinsic width to get a mass limit. We use this technique to search for phenomena including axigluons ($A \rightarrow q\overline{q}$) [12], Flavour Universal Colorons ($C \rightarrow q\overline{q}$) [13], excited states of composite quarks ($q^* \rightarrow qg$) [14], Color octet techni-ρ's ($\rho_T \rightarrow g \rightarrow q\overline{q}$,gg) [15], W', Z' bosons($W', Z' \rightarrow q\overline{q}$) [16], and E_6 diquarks ($D(D^c) \rightarrow \overline{q}\,\overline{q}(qq)$) [17]. No evidence for new particles is observed, and excluded mass regions for several models are drawn in Figure 13.

4.6 Search for new particles decaying to dileptons

Many extensions to the Standard Model predict extra neutral gauge bosons. Some examples of models that predict extra neutral gauge bosons are E_6 model Z's [18], and Randall-Sundrum gravitons [19]. For the most part these models do not constrain the masses of the neutral gauge bosons. 72 pb^{-1} of Run II data are used to search for extra neutral gauge bosons that decay to electrons and muons. The analyses require two high-p_T electrons or muons, and search the invariant mass spectrum above the Z pole for excesses above the Standard Model prediction. The observed dilepton mass spectra agree with the background

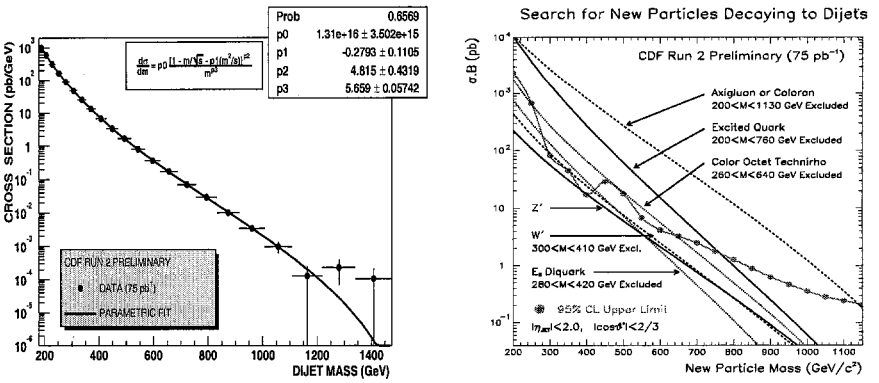

Fig. 13. A fit of the dijet mass distribution with 10% wide mass bins to a smooth function, where a deviation would indicate an excess in the cross section over the dijet mass spectrum(left). 95% CL upper limits on $\sigma \cdot \mathrm{Br}$ for new particles decaying to dijets (right).

expectation (Figure 14). A 95% CL upper limit on the production $\sigma \cdot \mathrm{Br}(\ell\ell)$ is set as a function of Z' mass and Randall-Sundrum graviton mass. A 95% CL lower limit on the Z' mass is established at 665 GeV/c^2 (Figure 15(left)), when Standard Model couplings are assumed. A 95% CL lower limit on the Randall-Sundrum graviton mass is made for various values of k/M_{Pl} (Figure 15(right)).

4.7 Search for new particles decaying to diphotons

In many models involving physics beyond the Standard Model, cascade decays of heavy new particles generate $\gamma\gamma$ signatures involving $\not\!\!E_T$, jets, leptons, gauge bosons (W, Z, γ), and possibly b-quarks. Some examples are supersymmetry with a light gravitino [20], radiative decays to a higgsino-LSP [21], and models with large symmetry groups [22]. This analysis begins a systematic search for anomalous $\gamma\gamma$ events such as the $ee\gamma\gamma\not\!\!E_T$ event found in Run I [23]. With 84 pb^{-1} of Run II data, we require 2 central photons ($E_T > 13$GeV), and find good agreement with Standard Model predictions. We compare the $\not\!\!E_T$and $M_{\gamma\gamma}$ distributions with the expected Standard Model production in Figure 16. No $\gamma\gamma\ell\ell$ events have yet been observed in Run II.

5 Prospects

The Run II dataset is approaching the size of the Run I dataset, and in many cases has the same physics reach, because of the increase in center of mass energy and improvements in the detector. Table 7 shows the expected event yields for each experiment with 2 fb^{-1} of data compared to the event samples from Run I. With 2 fb^{-1} of data we expect to be able to measure the W mass with an uncertainty of 40 MeV/c^2, and the top mass with an uncertainty of 3 GeV/c^2 ,

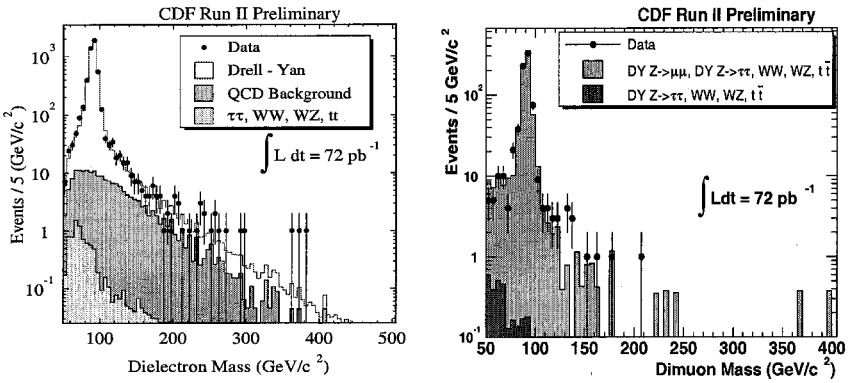

Fig. 14. The dielectron(left) and dimuon(right) mass spectrum from 72 pb^{-1} of Run II data compared with expected backgrounds. These spectra are used to search for extra neutral gauge bosons.

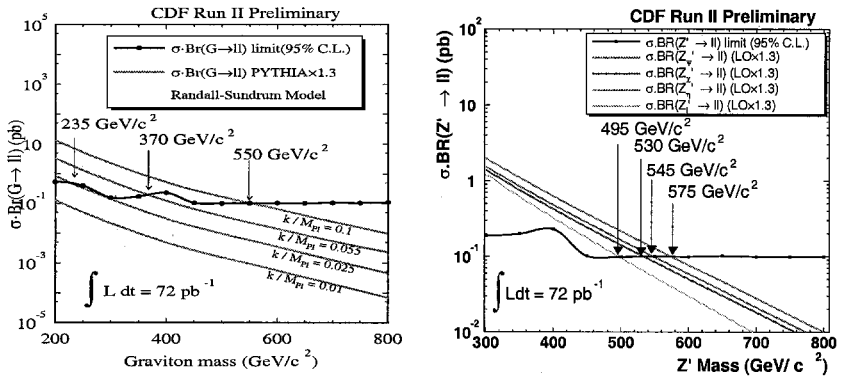

Fig. 15. 95% CL upper limit on $\sigma\cdot\text{Br}(\ell\ell)$ as a function of graviton mass compared with different values of k/M_{Pl}(left). 95% CL upper limit on $\sigma\cdot\text{Br}(\ell\ell)$ as a function of Z' mass compared with LO theoretical prediction for Z' (right).

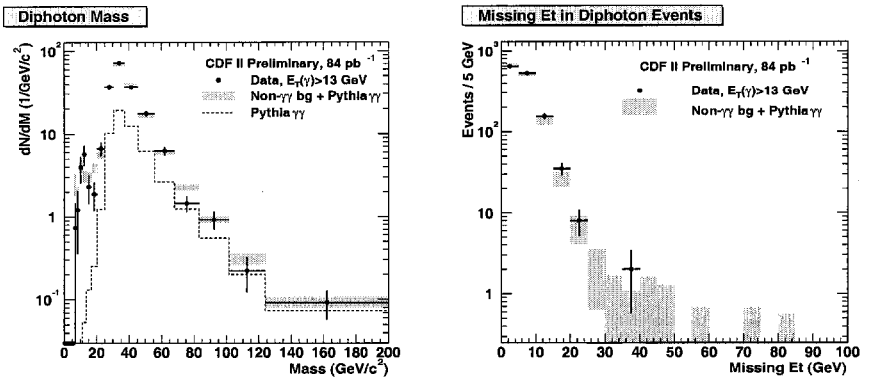

Fig. 16. Kinematic distributions from diphoton events in 84 pb^{-1} of Run II data compared with Standard Model backgrounds. The $\not\!\!E_T$(left) and $M_{\gamma\gamma}$ are distributions that might be sensitive to new physics beyond the Standard Model.

Table 7. Expected event yields per experiment with 2 fb^{-1} of data.

Sample	Run I	Run II
$W \to \ell\nu_\ell$	77,000	2,300,000
$Z \to \ell^+\ell^-$	10,000	202,000
WV ($W \to \ell\nu_\ell$,$V = W, \gamma, Z$)	90	1,800
ZV ($Z \to \ell^+\ell^-$,$V = W, \gamma, Z$)	30	500
$t\bar{t}$ (mass sample,≥ 1 b-tag)	20	800

further constraining electroweak fits for the Higgs mass. The enormous increase in the top samples will allow us for the first time to make precision measurements of top quark production and its properties. We will also be searching for new objects at and above the electroweak scale. We will be sensitive to charginos up to 130 GeV/c^2 , to gluinos up to 270 GeV/c^2 , stop quarks up to 150 GeV/c^2 , second generation lepto-quarks up to 300 GeV/c^2 , new vector bosons up to masses of 900 GeV/c^2 , and excited quarks up to 800 GeV/c^2 . We believe our prospects are best interpreted as a list of probable sensitivities to the real surprises that lie at the electroweak scale.

6 Conclusions

Run II at the Tevatron is well under way. The CDF experiment has reestablished many baseline electroweak measurements. The top program has been launched and will be an area of a lot of excitement in the next few years. We have also reestablished limits on new physics, many of which already improve on Run I results.

7 Acknowledgments

I would like to thank my CDF collaborators for their help in preparing this document. We thank the Fermilab staff and the technical staffs of the participating institutions for their vital contributions. This work was supported by the U.S. Department of Energy and National Science Foundation; the Italian Istituto Nazionale di Fisica Nucleare; the Ministry of Education, Culture, Sports, Science and Technology of Japan; the Natural Sciences and Engineering Research Council of Canada; the National Science Council of the Republic of China; the Swiss National Science Foundation; the A.P. Sloan Foundation; the Bundesministerium fuer Bildung und Forschung, Germany; the Korean Science and Engineering Foundation and the Korean Research Foundation ; the Particle Physics and Astronomy Research Council and the Royal Society, UK; the Russian Foundation for Basic Research; and the Comision Interministerial de Ciencia y Tecnologia, Spain.

References

1. A. D. Martin *et al.*, Phys. Lett. B **531**, 216 (2002), [arXiv:hep-ph/9905386]; W.J. Stirling, private communication.
2. A. Connolly [CDF Collaboration], [arXiv:hep-ex/0212016].
3. K. Hagiwara *et al.* [Particle Data Group Collaboration], Phys. Rev. D **66**, 010001 (2002).
4. J. L. Rosner, M. P. Worah and T. Takeuchi, Phys. Rev. D **49**, 1363 (1994), [arXiv:hep-ph/9309307].
5. M. Cacciari, S. Frixione, M. L. Mangano, P. Nason and G. Ridolfi, [arXiv:hep-ph/0303085].
6. U. Baur, M. Spira and P. M. Zerwas, Phys. Rev. D **42**, 815 (1990).
7. M. Kramer, T. Plehn, M. Spira and P. M. Zerwas, Phys. Rev. Lett. **79**, 341 (1997) [arXiv:hep-ph/9704322].
8. T. P. Cheng and L. F. Li, Phys. Rev. D **22**, 2860 (1980).
9. R. N. Mohapatra and J. C. Pati, Phys. Rev. D **11**, 566 (1975); G. Senjanovic and R. N. Mohapatra, Phys. Rev. D **12**, 1502 (1975); R. N. Mohapatra and G. Senjanovic, Phys. Rev. D **23**, 165 (1981).
10. C. S. Aulakh, A. Melfo and G. Senjanovic, Phys. Rev. D **57**, 4174 (1998) [arXiv:hep-ph/9707256]; Z. Chacko and R. N. Mohapatra, Phys. Rev. D **58**, 015003 (1998) [arXiv:hep-ph/9712359].
11. R. Barbieri, L. J. Hall and Y. Nomura, Phys. Rev. D **63**, 105007 (2001) [arXiv:hep-ph/0011311].
12. P. H. Frampton and S. L. Glashow, Phys. Lett. B **190**, 157 (1987); J. Bagger, C. Schmidt and S. King, Phys. Rev. D **37**, 1188 (1988).
13. R. S. Chivukula, A. G. Cohen and E. H. Simmons, Phys. Lett. B **380**, 92 (1996) [arXiv:hep-ph/9603311]; E. H. Simmons, Phys. Rev. D **55**, 1678 (1997) [arXiv:hep-ph/9608269].
14. U. Baur, I. Hinchliffe and D. Zeppenfeld, Int. J. Mod. Phys. A **2**, 1285 (1987); U. Baur, M. Spira and P. M. Zerwas, Phys. Rev. D **42**, 815 (1990).
15. K. D. Lane and M. V. Ramana, Phys. Rev. D **44**, 2678 (1991); E. Eichten and K. D. Lane, Phys. Lett. B **327**, 129 (1994) [arXiv:hep-ph/9401236].
16. F. Abe *et al.* [CDF Collaboration], Phys. Rev. Lett. **74**, 2900 (1995) and F. Abe *et al.* [CDF Collaboration] and Phys. Rev. D **51**, 949 (1995), and references therein.

17. J. L. Hewett and T. G. Rizzo, Phys. Rept. **183**, 193 (1989).
18. J. L. Hewett and T. G. Rizzo, Phys. Rept. **183**, 193 (1989); A. Leike, Phys. Rept. **317**, 143 (1999) [arXiv:hep-ph/9805494].
19. L. Randall and R. Sundrum, Phys. Rev. Lett. **83**, 4690 (1999) [arXiv:hep-th/9906064]; L. Randall and R. Sundrum, Phys. Rev. Lett. **83**, 3370 (1999) [arXiv:hep-ph/9905221].
20. M. Dine, A. E. Nelson, Y. Nir and Y. Shirman, Phys. Rev. D **53**, 2658 (1996) [arXiv:hep-ph/9507378]; S. Dimopoulos, M. Dine, S. Raby and S. Thomas, Phys. Rev. Lett. **76**, 3494 (1996) [arXiv:hep-ph/9601367]; S. Dimopoulos, S. Thomas and J. D. Wells, Phys. Rev. D **54**, 3283 (1996) [arXiv:hep-ph/9604452]; K. S. Babu, C. F. Kolda and F. Wilczek, Phys. Rev. Lett. **77**, 3070 (1996) [arXiv:hep-ph/9605408]; J. L. Lopez and D. V. Nanopoulos, Mod. Phys. Lett. A **10**, 2473 (1996) [arXiv:hep-ph/9607220]; S. Ambrosanio, G. L. Kane, G. D. Kribs, S. P. Martin and S. Mrenna, Phys. Rev. D **54**, 5395 (1996) [arXiv:hep-ph/9605398]; J. A. Bagger, K. T. Matchev, D. M. Pierce and R. j. Zhang, Phys. Rev. D **55**, 3188 (1997) [arXiv:hep-ph/9609444]; H. Baer, M. Brhlik, C. h. Chen and X. Tata, Phys. Rev. D **55**, 4463 (1997) [arXiv:hep-ph/9610358].
21. H. E. Haber, G. L. Kane and M. Quiros, Phys. Lett. B **160**, 297 (1985); S. Ambrosanio, G. L. Kane, G. D. Kribs, S. P. Martin and S. Mrenna, Phys. Rev. Lett. **76**, 3498 (1996) [arXiv:hep-ph/9602239]; S. Ambrosanio, G. L. Kane, G. D. Kribs, S. P. Martin and S. Mrenna, Phys. Rev. D **55**, 1372 (1997) [arXiv:hep-ph/9607414].
22. G. Bhattacharyya and R. N. Mohapatra, Phys. Rev. D **54**, 4204 (1996) [arXiv:hep-ph/9606408]; J. L. Rosner, Phys. Rev. D **55**, 3143 (1997) [arXiv:hep-ph/9607467]; K. D. Lane, Phys. Lett. B **357**, 624 (1995) [arXiv:hep-ph/9507289].
23. S. Park, Proceedings of the 10th Topical Workshop on Proton-Antiproton Collider Physics, R. Raja and J. Yoh, eds., AIP press, May 1995, p. 62.